International Journal of Solids and Structures 46 (2009) 2800–2808

Contents lists available at ScienceDirect

International Journal of Solids and Structures

journal homepage: www.elsevier.com/locate/ijsolstr

Buckling analysis of imperfect shells with stochastic non-Gaussian material and thickness properties

Vissarion Papadopoulos, George Stefanou *, Manolis Papadrakakis

Institute of Structural Analysis & Seismic Research, National Technical University of Athens, 9, Iroon Polytechniou Str., Zografou Campus, GR-15780 Athens, Greece

ARTICLE INFO

Article history:
Received 28 December 2008
Received in revised form 25 February 2009
Available online 24 March 2009

Keywords:
Nonlinear shell finite element
Buckling analysis
Random imperfections
Non-Gaussian stochastic fields
Spectral representation

ABSTRACT

In this paper, the effect of material and thickness spatial variation on the buckling load of isotropic shells with random initial geometric imperfections is investigated. To this purpose, a random spatial variability of the elastic modulus as well as of the thickness of the shell is introduced in addition to the random initial geometric deviations of the shell structure from its perfect geometry. The main novelty of this paper compared to previous works is that a non-Gaussian assumption is made for the distribution of the two aforementioned uncertain parameters i.e. the modulus of elasticity and the shell thickness which are described by two-dimensional uni-variate (2D-1V) homogeneous non-Gaussian stochastic fields. The initial geometric imperfections are described as a 2D-1V Gaussian non-homogeneous stochastic field with properties derived from corresponding experimental measurements. Numerical examples are presented focusing on the influence of the non-Gaussian assumption on the variability of the buckling load, which is calculated by means of the Monte Carlo Simulation method. It is shown that the choice of the marginal probability distribution for the description of the material and thickness variability is crucial since it affects significantly the statistics of the buckling load of imperfection sensitive shell-type structures.

1. Introduction

The analysis and design of imperfection sensitive shells had always an appeal to structural engineers and constitute the subject of extensive research. The main issue when dealing with this problem is the big discrepancy between theory and experiment as well as the large scatter in the measured buckling loads. Both deterministic and probabilistic approaches have been used to address the aforementioned issues. It was soon realized that the problem could only be addressed through modeling taking into account the randomness of the imperfect geometries (Chryssanthopoulos and Poggi, 1995; Deml and Wunderlich, 1997; Schenk and Schuëller, 2003). Additional research revealed that, other sources of imperfections such as the variability of thickness, material properties, boundary conditions and misalignment of loading are also responsible for the reduction and scatter of the buckling load of shell structures (Palassopoulos, 1993; Morris, 1996; Elishakoff, 2000; Elishakoff et al., 2001; Arbocz and Starnes, 2002; Tsouvalis et al., 2003; Ikeda and Murota, 2008).

Even though the reasons of the discrepancy and the scatter of the buckling loads were clearly understood and demonstrated many years ago, it is only the last five to ten years that researchers focused on the combined effect of additional sources of imperfections with the initial geometric ones. It is nowadays generally recognized that an accurate prediction of the buckling behavior of shells requires a realistic description of all uncertainties involved in the problem and that such task is realizable only in the framework of a robust Stochastic Finite Element Method (SFEM) formulation that can efficiently and accurately handle geometric as well as physical nonlinearities of shell-type structures (Choi and Noh, 2000; Graham and Siragy, 2001; Argyris et al., 2002b; Papadopoulos and Papadrakakis, 2004, 2005; Stefanou and Papadrakakis, 2004; Lagaros and Papadopoulos, 2006; Noh, 2006; Onkar et al., 2006; Papadopoulos and Iglesis, 2007). The analysis of such structures has been carried out in a probabilistic context through the application of the Finite Element method in conjunction with the Monte Carlo Simulation, incorporating realistic descriptions of the uncertainties involved in geometric (Bielewicz and Górski, 2002; Schenk and Schuëller, 2003), material and thickness imperfections (Papadopoulos and Papadrakakis, 2004, 2005), as well as boundary conditions (Papadopoulos and Iglesis, 2007; Schenk and Schuëller, 2007). All these uncertainties were modeled as stochastic fields using either the Karhunen–Loève expansion or the spectral representation method.

In the present paper, the effect of combined geometric, boundary, material and thickness variations on the buckling load of a thin isotropic axially compressed imperfect cylinder is re-evaluated with respect to previous works, taking into account additional

* Corresponding author.
E-mail addresses: vpapado@central.ntua.gr (V. Papadopoulos), stegesa@central.ntua.gr (G. Stefanou), mpapadra@central.ntua.gr (M. Papadrakakis).

0020-7683/$ - see front matter © 2009 Elsevier Ltd. All rights reserved.
doi:10.1016/j.ijsolstr.2009.03.006

sensitivities due to various non-Gaussian assumptions. To this purpose, a non-Gaussian spatial variability of the elastic modulus as well as of the thickness of the shell is introduced in addition to the random initial (out-of-plane) geometric and boundary (in-plane edge) imperfections. Following an approach similar to that used in Papadopoulos and Papadrakakis (2005), out-of-plane initial geometric imperfections are modeled as a 2D-1V non-homogeneous Gaussian stochastic field, with properties derived from corresponding experimental measurements (Arbocz and Abramovich, 1979). The uncertain boundary in-plane imperfections are taken into account through modeling a stochastic non-uniform axial loading, described by a 1D-1V homogeneous Gaussian stochastic field and applied as incremental load in the nonlinear analysis. As shown in detail in Papadopoulos and Iglesis (2007), the aforementioned approach is essentially equivalent to modeling the boundary imperfections in the sense that both of them result in a non-uniform axial load pattern acting on the cylinders' edges introducing this way an in-plane edge imperfection pattern (Arbocz, 2000; Schenk and Schuëller, 2007).

The modulus of elasticity and the shell thickness are described by 2D-1V uncorrelated homogeneous non-Gaussian stochastic fields using the spectral representation method in conjunction with the translation field theory (Shinozuka and Deodatis, 1996; Grigoriu, 1984, 1998). Translation-based approaches (Deodatis and Micaletti, 2001; Lagaros et al., 2005) that make use of an extended empirical non-Gaussian to non-Gaussian mapping for the generation of a non-Gaussian field, having the prescribed characteristics (target marginal distribution and spectral density function), are also evaluated. The numerical example presented herewith focuses on the relative influence of the non-Gaussian assumption (a lognormal and three different beta distributions are used) on the variability of the buckling load, which is calculated by means of the Monte Carlo Simulation (MCS) method. For the determination of the limit load of the shell, a stochastic formulation of the geometrically nonlinear elastoplastic facet triangular shell element TRIC based on the midpoint method, is implemented (Argyris et al., 1998, 2002a). Results are presented for an axially compressed thin-walled cylinder. These results are compared to corresponding experimental measurements and it is shown that the choice of the marginal probability distribution for the description of the material and thickness variability is crucial since it affects significantly the statistics of the buckling load of imperfection sensitive shell-type structures.

2. Finite element formulation – the TRIC shell element

The finite element simulation is performed using the nonlinear multilayer triangular shell element TRIC, which is based on the natural mode method. The TRIC shear-deformable facet shell element is a reliable and cost-effective element suitable for linear and nonlinear analysis of thin and moderately thick isotropic as well as composite plate and shell structures. The element has 18 degrees of freedom (6 per node) and hence 12 natural straining modes. Three natural axial strains and natural transverse shear strains are measured parallel to the edges of the triangle. The natural stiffness matrix is derived from the statement of variation of the strain energy with respect to the natural coordinates. The geometric stiffness is based on large deflections but small strains. In the case of material nonlinearity, the elastoplastic constitutive matrix is established by obtaining the relation between the natural strain and stress increments for each layer within a given load step. The natural elastoplastic stiffness of the element is obtained by summing up the natural elastoplastic stiffnesses of the element layers. A detailed description of the linear elastic, geometric and elastoplastic stiffness matrix of the TRIC shell element can be found in Argyris et al. (2002b, 1998, 2002a), respectively.

3. Out-of-plane initial geometric imperfections

For the axially compressed cylinder of Fig. 1, out-of-plane initial geometric imperfections are modeled as a 2D non-homogeneous Gaussian stochastic field. The mean material and geometric properties of the perfect cylinder are shown in Fig. 1. Following a procedure similar to that used in Papadopoulos and Papadrakakis (2005), the mean values as well as the evolutionary power spectra of the aforementioned non-homogeneous fields are derived from corresponding experimental measurements.

The imperfect geometry of the shell is represented by the spatial variation of the radius of the structure as follows:

$$r(x,y) = R + a_0(x,y) + g_1(x,y) \tag{1}$$

where $r(x,y)$ is the varying initial radius at each point of the structure, R is the radius of the perfect cylinder, $a_0(x,y)$ is the mean function of the imperfections with respect to the perfect geometry of the shell and $g_1(x,y)$ is a zero-mean non-homogeneous Gaussian stochastic field.

The mean function $a_0(x,y)$ as well as the properties of stochastic field $g_1(x,y)$ are derived from a statistical analysis of experimentally measured imperfections on seven copper electroplated cylindrical shells, named as A-shells, contained in a data bank of initial imperfections (Arbocz and Abramovich, 1979). The geometric and material properties of the perfect configurations of these shells as well as the corresponding experimental buckling loads are presented in Table 1. More details on the statistical description of the out-of plane initial geometric imperfections are provided in Appendix A.

4. Stochastic stiffness matrix

The modulus of elasticity and the thickness of the shell are also considered in the present study as "imperfections", due to their spatial variability. These parameters are described by two uncorrelated 2D-1V homogeneous non-Gaussian stochastic fields:

$$E(x,y) = E_0[1 + f_1(x,y)] \tag{2}$$

$$t(x,y) = t_0[1 + f_2(x,y)] \tag{3}$$

where E_0 is the mean value of the elastic modulus, t_0 is the mean thickness of the structure and $f_1(x,y)$, $f_2(x,y)$ are two zero-mean non-Gaussian homogeneous stochastic fields corresponding to the

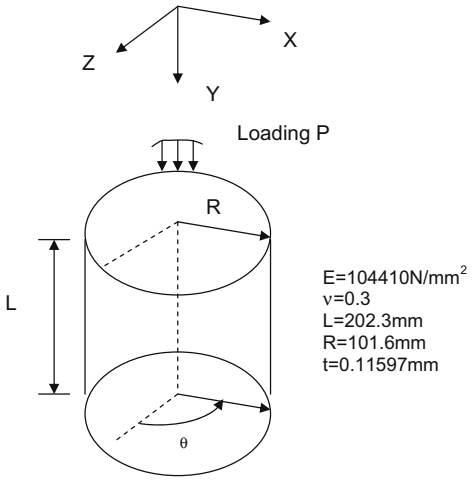

Fig. 1. Geometry and material data of the axially compressed cylinder.

Table 1
Geometry, material properties and experimental buckling loads of A-shells.

Shell	R (mm)	t (mm)	L (mm)	E (N/mm^2)	P (N)
A-7	101.6	0.1140	203.20	104110	3036.4
A-8	101.6	0.1179	203.20	104800	3673.8
A-9	101.6	0.1153	203.20	101350	3724.8
A-10	101.6	0.1204	203.20	102730	3196.9
A-12	101.6	0.1204	209.55	104800	3853.0
A-13	101.6	0.1128	196.85	104110	3108.8
A-14	101.6	0.1110	196.85	108940	3442.9

variability of the modulus of elasticity and the thickness of the shell, respectively. The stochastic stiffness matrix of the shell element is derived using the midpoint method i.e. one integration point at the centroid of each finite element is used for the computation of the stiffness matrix.

5. Simulation of non-Gaussian material and thickness imperfections

As mentioned in the previous section, a non-Gaussian assumption is made for the distribution of material and thickness imperfections. The problem of simulating non-Gaussian stochastic processes and fields has recently received considerable attention in the field of stochastic mechanics. This is due to the fact that several quantities arising in practical engineering problems (e.g. material and geometric properties of structural systems, soil properties, wind loads, waves) are found to exhibit non-Gaussian probabilistic characteristics.

Since all the joint multi-dimensional density functions are needed to fully characterize a non-Gaussian stochastic field, a number of studies have been focused on producing a more realistic definition of a non-Gaussian sample function from a simple transformation of some underlying Gaussian field with known second-order statistics. Thus, if $g(\mathbf{x})$ is a homogeneous zero-mean Gaussian field with unit variance and spectral density function (SDF) $S_{gg}(\boldsymbol{\kappa})$ (or equivalently autocorrelation function $R_{gg}(\xi)$), a homogeneous non-Gaussian stochastic field $f(\mathbf{x})$ with power spectrum $S_{ff}^{T}(\boldsymbol{\kappa})$ can be defined as:

$$f(\mathbf{x}) = F^{-1} \cdot \Phi[g(\mathbf{x})] \tag{4}$$

where Φ is the standard Gaussian cumulative distribution function and F is the non-Gaussian marginal cumulative distribution function of $f(\mathbf{x})$. The transform $F^{-1} \cdot \Phi$ is a memory-less translation since the value of $f(\mathbf{x})$ at an arbitrary point $\mathbf{x}$ depends on the value of $g(\mathbf{x})$ at the same point only and the resulting non-Gaussian field is called a translation field (Grigoriu, 1984, 1998).

The main shortcoming of translation fields is that, although the mapped sample functions of Eq. (4) will have the prescribed target marginal probability distribution F, their SDF will not be identical to $S_{ff}^{T}(\boldsymbol{\kappa})$. Another important issue, pointed out by Grigoriu (1998), is that the choice of the marginal distribution of $f(\mathbf{x})$ imposes constraints to its correlation structure. In other words, F and $S_{ff}^{T}(\boldsymbol{\kappa})$ (or $R_{ff}^{T}(\xi)$) have to satisfy a specific compatibility condition derived directly from the definition of the autocorrelation function of the translation field:

$$R_{ff}^{T}(\xi) = \int_{-\infty}^{\infty}\int_{-\infty}^{\infty} F^{-1}[\Phi(g_1)]F^{-1}[\Phi(g_2)] \cdot \phi[g_1, g_2; R_{gg}(\xi)]dg_1 dg_2 \tag{5}$$

where $\phi[g_1,g_2;R_{gg}(\xi)]$ denotes the joint density of $\{g_1,g_2\}$ and $g_1 = g(\mathbf{x})$, $g_2 = g(\mathbf{x}+\xi)$. If these two quantities are proven to be incompatible through Eq. (5) i.e. if $R_{ff}^{T}(\xi)$ has certain values lying outside a range of admissible values and/or the solution $R_{gg}(\xi)$ is not positive definite and therefore not admissible as an autocorrelation function, there is no translation field with the prescribed characteristics. In this case, one has to resort to translation fields that match the target marginal distribution and/or SDF approximately. At this point, it must be noted that translation fields have a number of useful properties such as the analytical calculation of crossing rates and extreme value distributions.

The two aforementioned problems arising in the context of translation fields are treated in (Deodatis and Micaletti, 2001; Lagaros et al., 2005) by using (i) an iterative procedure involving the repeated updates of the SDF of the underlying Gaussian stochastic field $g(\mathbf{x})$ and, (ii) an extended empirical non-Gaussian to non-Gaussian mapping leading to the generation of a non-Gaussian field $f(\mathbf{x})$ with the prescribed F and $S_{ff}^{T}(\boldsymbol{\kappa})$:

$$f(\mathbf{x}) = F^{-1} \cdot F^{*}[g(\mathbf{x})] \tag{6}$$

where F^{*} is the empirical marginal probability distribution of $g(\mathbf{x})$ updated at each iteration.

The iterative updating procedure is defined in such a way that when the final realization of $g(\mathbf{x})$ is generated, according to the updated $S_{gg}(\boldsymbol{\kappa})$ and then mapped to $f(\mathbf{x})$ via Eq. (6), the resulting non-Gaussian sample function will have the prescribed marginal probability distribution as well as SDF. Sample functions of $g(\mathbf{x})$ are generated using the spectral representation method. The extended empirical non-Gaussian to non-Gaussian mapping of Eq. (6) is used in order to overcome the inherent limitations associated with the translation field concept, namely the possible incompatibility between the marginal distribution and the correlation structure of a translation field. Since experimental data can lead to a theoretically incompatible pair of F and $S_{ff}^{T}(\boldsymbol{\kappa})$, it is obvious that an algorithm covering a wider range of non-Gaussian fields is of great practical interest.

In the present work, Eq. (4) is directly used for the generation of non-Gaussian translation sample functions since there are no experimental data imposing a specific pair of $F - S_{ff}^{T}(\boldsymbol{\kappa})$ and a translation field is preferable to use. The SDF $S_{gg}(\boldsymbol{\kappa})$ of the underlying Gaussian field used in the numerical examples (Section 7) is assumed to correspond to an autocorrelation function of square exponential type and is given by:

$$S_{gg}(\kappa_1, \kappa_2) = \sigma_g^2 \frac{b_1 b_2}{4\pi} \exp\left[-\frac{1}{4}(b_1^2\kappa_1^2 + b_2^2\kappa_2^2)\right] \tag{7}$$

where σ_g denotes the standard deviation of the stochastic field and b_1, b_2 denote the parameters that influence the shape of the spectrum which are proportional to the correlation lengths of the stochastic field along the x and y axes, respectively. The SDF of the translation field obtained from Eq. (4) is different from $S_{gg}(\boldsymbol{\kappa})$ as it is shown in the section of numerical examples.

Using the procedure described in this section, a large number N_{SAMP} of non-Gaussian sample functions are produced, leading to the generation of a set of stochastic stiffness matrices. The associated structural problem is solved N_{SAMP} times and the response variability can finally be calculated by obtaining the response statistics of the N_{SAMP} simulations.

6. Non-uniformity of axial loading

A simple and realistic approach is used for the treatment of edge imperfections by assuming that these are produced by a non-uniform random axial load distribution that can be modeled as a 1D homogeneous stochastic field assigning an equivalent concentrated force at each node of the discretized cylinder's edge, as follows:

$$P(x) = P_0[1 + g_2(x)] \tag{8}$$

where P_0 is the fixed (mean) value of the vertical applied load increment and $g_2(x)$ is a zero-mean Gaussian homogeneous stochastic

field modeled with a two-sided SDF corresponding to an autocorrelation function of square exponential type:

$$S_{gg}(\kappa) = \frac{\sigma_g^2}{4\pi} b_g \exp\left[-\frac{1}{4}(b_g^2\kappa^2)\right] \quad (9)$$

Thus, an edge deformation pattern is obtained at the beginning of the incremental nonlinear analysis procedure, which is assumed to correspond to the actual edge imperfections' pattern. Some remarks on the validity of the procedure for modeling the uncertain boundary conditions can be found in Appendix B.

7. Numerical examples

A numerical implementation of the above described methodology is presented for the axially compressed cylinder of Fig. 1. The boundary conditions are specified as follows: the base edge nodes of the cylinder are fixed against all translations, fixed against rotations around the Y axis and free against rotations around the X and Z axis. The top edge nodes of the cylinder are fixed against X and Z translations, fixed against rotations around the Y axis, free against translations in the Y axis and free against rotations around axis X and Z.

Mesh convergence studies were performed by Schenk and Schuëller (2003), Papadopoulos and Papadrakakis (2005) in order to determine an optimum FE mesh size satisfying the following two requirements: (i) accurate prediction of the buckling load of the cylinder and, (ii) accurate representation of the gradients of the stochastic initial imperfection field. In these convergence studies, it has been observed that a coarse mesh of 51×101 produces a very small ($\sim$1%) relative discretization error of the buckling loads with respect to buckling loads calculated with more refined meshes. In addition, this mesh size provides a sufficiently accurate representation of the gradients of the imperfect shape of the cylinder since it is a fraction of the correlation lengths of the stochastic fields used for both axial and circumferential directions (Li and Der Kiureghian, 1992). For comparison purposes, all loads are normalized with respect to the buckling load of the perfect cylinder calculated using the mesh of 51×101, which is found to be $P_u^{(\text{perfect})} = 5350$ N.

7.1. Effect of random geometric, boundary, material and thickness imperfections considered as stand-alone cases

As a first step of the numerical investigation, each source of imperfections is introduced separately in the axially compressed cylinder in order to examine the relative effect of randomness in the different quantities considered as stand-alone cases. Figs. 2(a) and (b) depict the results for the mean value and the coefficient of variation (Cov) of the computed buckling loads as a function of the imperfection type, for two different correlation length parameters $b_1 = b_2 = 50$ mm and $b_1 = b_2 = 500$ mm, respectively. It can be seen that the largest Cov($\approx$22%) of the buckling load P_u is obtained

Table 2
Range of definition and shape parameters of lognormal and beta distributions.

	Lower bound	Upper bound	Shape parameters	
Lognormal	−1	+∞	–	–
Beta – Case 1	−0.5	0.5	$p = 12$	$q = 12$
U-beta – Case 2	−0.16	0.16	$p = 0.8$	$q = 0.8$
L-beta – Case 3	−0.13	0.26	$p = 0.8$	$q = 1.6$

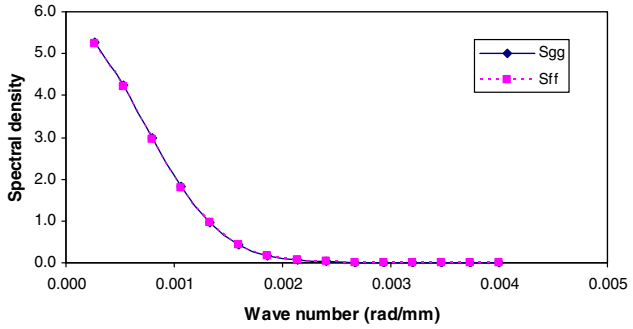

Fig. 3. Ensemble SDF of the lognormal translation field (1000 simulations) and square exponential SDF of the underlying Gaussian field in one dimension for $\sigma = 10\%$, $b = 2000$ mm.

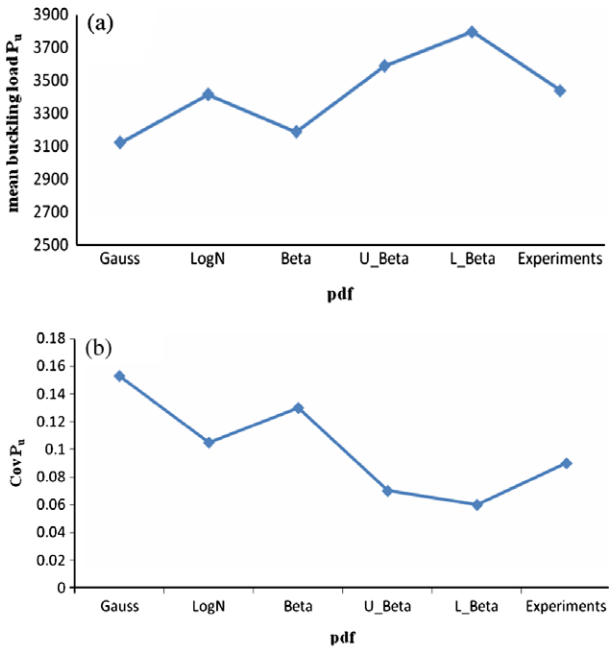

Fig. 4. (a) Mean value and (b) coefficient of variation of the computed buckling loads as a function of the marginal pdf used for the description of the material and thickness imperfections.

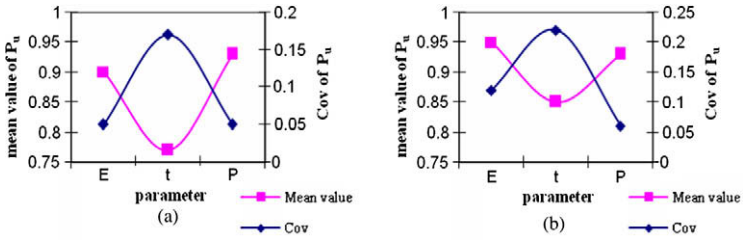

Fig. 2. Mean value and coefficient of variation (Cov) of the normalized buckling load P_u in the case of uncertain Young modulus E, thickness t and non-uniform axial loading P for correlation length parameters (a) $b = 50$ mm and (b) $b = 500$ mm.

in the case of thickness variation (σ_g = 10%) and b = 500 mm. In this case, a large magnification of uncertainty occurs, as the response Cov value is about two times greater than that of the input Cov. It thus seems that thickness imperfections are predominant but the other quantities have also a significant effect on the buckling load variability: a Young modulus variation with σ_g = 10% leads to Cov($-P_u$) ≈ 11% while the boundary imperfections with σ_g = 10% lead to Cov(P_u) ≈ 6.5%. Concerning the random out-of-plane geometric

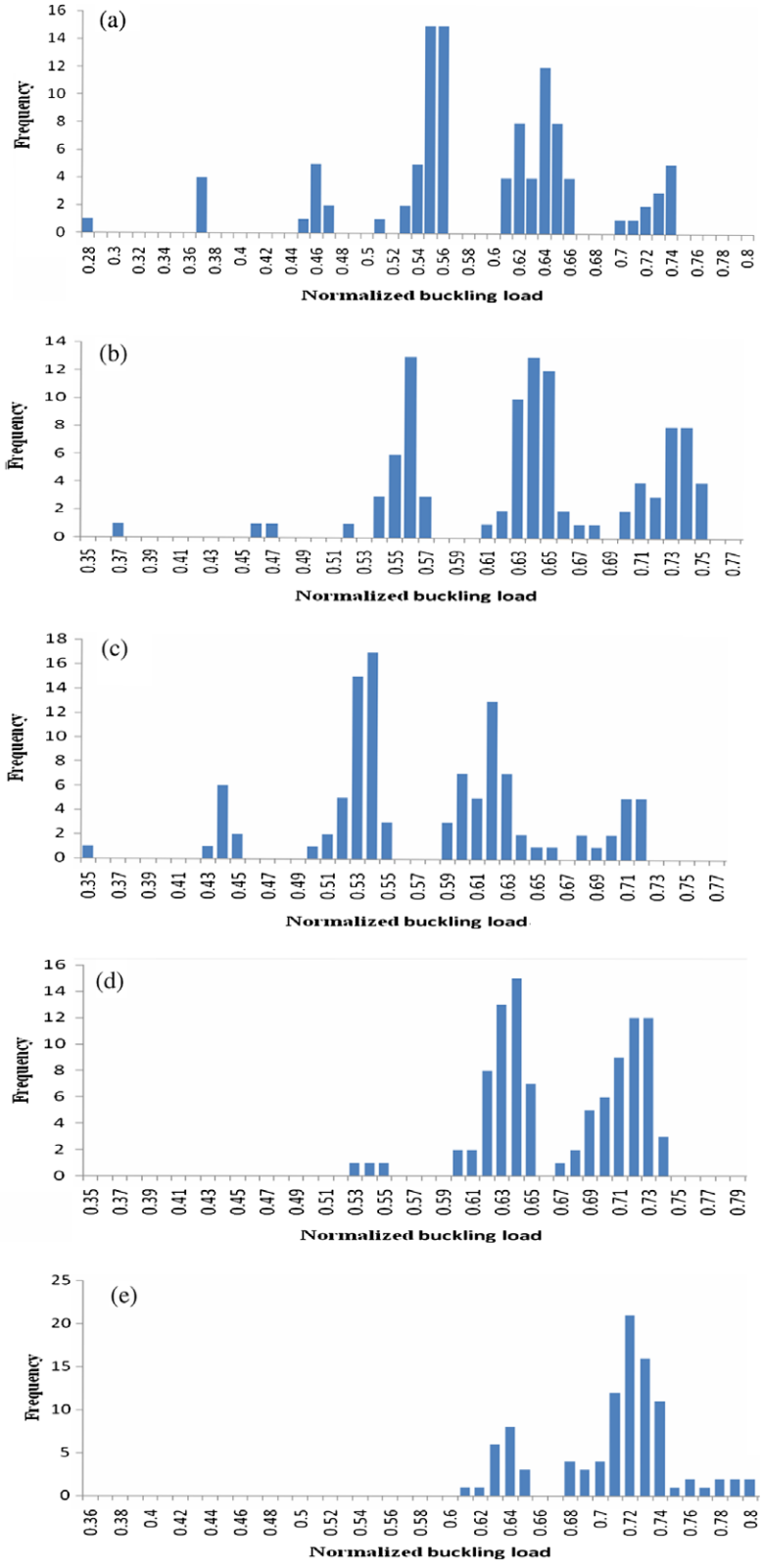

Fig. 5. Combined geometric, boundary, material and thickness imperfections: histogram of critical load factors (a) Gaussian, (b) lognormal, (c) beta, (d) U-shaped beta and (e) L-shaped beta description of the material and thickness imperfections.

imperfections, the corresponding Cov was computed in Papadopoulos and Papadrakakis (2005) at 7.5% with a mean value of the normalized buckling load equal to 0.90. The above results have been obtained using Gaussian stochastic fields for the description of all the involved uncertain quantities. The corresponding calculations using a non-Gaussian assumption for the elastic modulus and thickness (with the same standard deviation $\sigma_f = 10\%$) resulted in practically the same values for the mean and Cov of the computed buckling loads with those presented in Fig. 2. The details of the various non-Gaussian distributions used are shown in Table 2. It is worth noting that although the largest Cov values are obtained for correlation length parameters $b_1 = b_2 = 500$ mm, the values $b_1 = b_2 = 50$ mm are responsible for the minimum mean values of the buckling load as shown in Fig. 2(a). For this reason, these values are selected for the description of the stochastic fields modeling the Young modulus and thickness in all subsequent applications since it is more likely to lead to "worst case" scenarios with respect to lowest buckling loads.

7.2. Combined geometric, boundary, material and thickness imperfections

The material and thickness imperfections as well as the initial out-of-plane geometric imperfections and imperfections of the boundary conditions are now simultaneously introduced to the model. Based on the results of previous work (Papadopoulos and Iglesis, 2007), the correlation length parameter $b_g = 100$ mm with $\sigma_g = 0.05$ is selected for the description of the stochastic field $g_2(x)$ used to model the load distribution on the upper edge of the cylinder (boundary imperfections) while, as described in Section 3, initial out-of-plane imperfections are modeled according to Eq. (1) as a non-homogeneous 2D stochastic field with statistical properties that are derived from corresponding experimental measurements.

As mentioned previously, the novelty of the present work compared to (Papadopoulos and Papadrakakis, 2004, 2005), is that a non-Gaussian assumption is made for the distribution of the Young modulus and shell thickness. A lognormal and three different cases of beta distribution with zero mean and $\sigma_f = 0.10$ are assumed to describe the variation of the two uncertain properties. The parameters of the aforementioned distributions are presented in Table 2. Sample functions of the corresponding stochastic fields are generated using Eqs. (2)–(4). A 1D plot of the ensemble SDF of the lognormal translation field (obtained from 1000 simulations) is given in Fig. 3 together with the square exponential SDF of the underlying Gaussian field. The differences between the two spectra are almost negligible in this case. Monte Carlo Simulation (MCS) with sample size $N_{SAMP} = 100$ is used for the calculation of the buckling load variability. As explained in the previous sub-section, the correlation length parameters $b_1 = b_2 = 50$ mm are selected for the description of the modulus of elasticity and thickness in all cases examined.

Figs. 4(a) and (b) present the mean value and the coefficient of variation (Cov) of the computed buckling loads, respectively, for each one of the examined marginal probability density functions (pdf) as well as the corresponding experimental results. From these figures, it can be observed that the choice of pdf plays a significant role on first and second order properties of the buckling load distribution. The largest Cov(=0.16) of the computed buckling loads corresponds to a Gaussian marginal pdf (mean $P_u = 3100$ N), while the lowest Cov(=0.06) corresponds to an L-shaped beta distribution (mean $P_u = 3800$ N). All other pdfs produce intermediate results that seem to be in better agreement with the experiments. It is worth noting that the Cov in all cases is smaller than that obtained when considering a stochastic variation of the shell thickness only.

Figs. 5 and 6 present the histograms of the computed and experimental buckling loads, respectively. From these figures, it can also be observed that the choice of pdf significantly affects the shape as well as the extreme values of the buckling load distribution. It can be seen that the lognormal and beta non-Gaussian assumption produce estimates of the scatter of the buckling load closer to the experimental measurements in comparison to the histograms obtained with the other pdf cases (Gaussian, U- and L-shaped beta). This is also illustrated with the quantile–quantile plots of Fig. 7. Although the number of experimental measurements is relatively small to reach safe conclusions regarding the shape of the distributions, it can be seen that the tri-modal shape of buckling loads observed in the experiments is represented in the corresponding numerical simulations. The minimum values of the lowest buckling load are provided by the Gaussian and beta pdfs and represent only the 28% and 35% of the buckling load of the perfect shell, respectively.

8. Conclusions

The effect of non-Gaussian material and thickness variability on the buckling load of isotropic cylindrical shells with random initial geometric and boundary imperfections has been investigated. The modulus of elasticity and the shell thickness were described by uncorrelated homogeneous non-Gaussian translation fields. A detailed analysis with respect to various non-Gaussian marginal pdfs of the material and thickness imperfections has been conducted. As a result of this analysis, it has been shown that the choice of the marginal pdf of the two uncertain parameters is crucial since it affects significantly the statistics of the buckling load. The largest Cov(=0.16) of the computed buckling loads corresponded to a Gaussian marginal pdf while the lowest Cov(=0.06) corresponded to an L-shaped beta distribution. All other pdfs produced intermediate results that seemed to be in better agreement with the experiments. It is worth noting that the Cov in all cases is smaller than that ob-

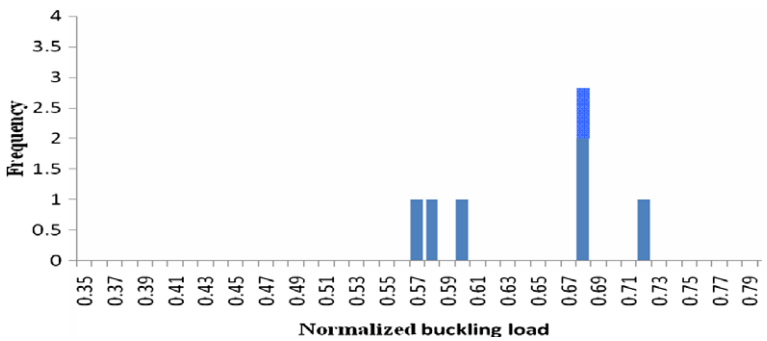

Fig. 6. Experimental results from seven specimens in Koiter (1963).

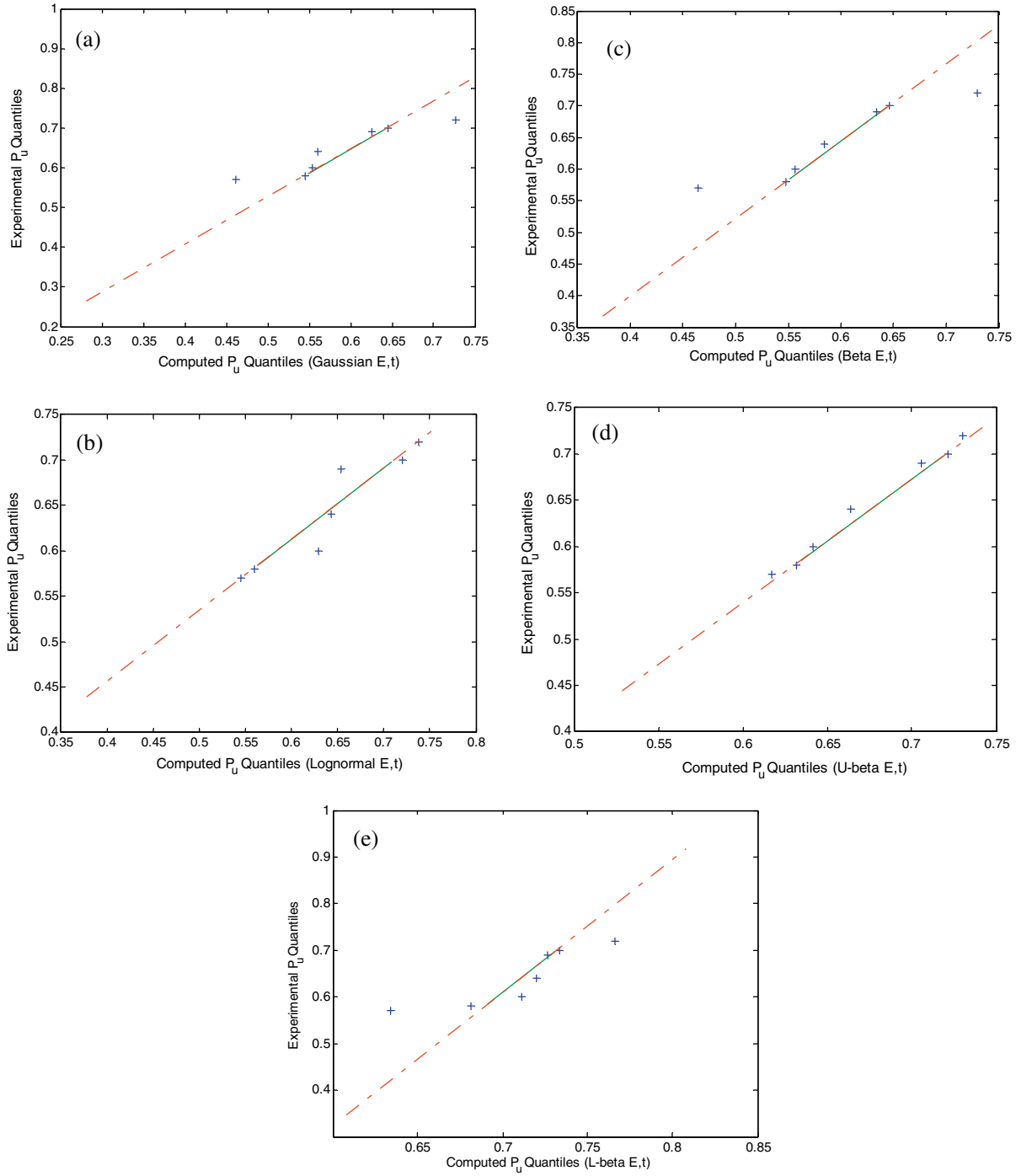

Fig. 7. Quantile–quantile plots of the experimental and computed buckling loads (a) Gaussian, (b) lognormal, (c) beta, (d) U-shaped beta and (e) L-shaped beta description of the material and thickness imperfections.

tained when considering a stochastic variation of the shell thickness only. A large magnification of uncertainty has been observed in the Gaussian case where the Cov of the ultimate load is 1.6 times higher than the Cov of material and thickness imperfections. From the histograms of the computed and experimental buckling loads, it has also been observed that the choice of pdf significantly affects the shape as well as the extreme values of the buckling load distribution. The lognormal and beta non-Gaussian assumptions led to estimates of the scatter of the buckling load closer to the experimental measurements in comparison to the results obtained with the other pdf cases (Gaussian, U- and L-shaped beta). Although the number of experimental measurements is relatively small to reach safe conclusions regarding the shape of the distributions, the tri-modal shape of buckling loads observed in the experiments has been reproduced by the corresponding numerical simulations. Finally, the lowest buckling load has been found to represent only the 28–60% of the buckling load of the perfect shell for the various cases of marginal pdfs considered.

Acknowledgements

This work has been partially supported by the research project "Konstantinos Karatheodori" of the National Technical University of Athens. This support is gratefully acknowledged.

Appendix A

A.1. Statistical description of out-of plane initial geometric imperfections

A typical pattern of measured out-of-plane geometric imperfections $w(x,y)$ is plotted in Fig. 8 for the A7 shell specimen of the data bank. It is evident that the corresponding 2D stochastic field is non-homogeneous with substantially varying first and second order properties. The mean function $a_0(x,y)$ is calculated via ensemble averaging at each point of the unfolded cylinder. A plot of $a_0(x,y)$ is presented in Fig. 9. The evolutionary power spectrum used for modeling the stochastic field $g_1(x,y)$ of Eq. (1) is written in the following form:

$$S^E(\kappa_x,\kappa_y,x,y) = S_x^E(\kappa_x,x)S_y^E(\kappa_y,y) \tag{A1}$$

where $S_x^E(\kappa_x,x)$ and $S_y^E(\kappa_y,y)$ are two independent 1D power spectra for the axial and circumferential direction, respectively. These power spectra are obtained using a windows sampling procedure. The separate evolutionary 1D spectra are evaluated over each sample and averaged over the ensemble. The length of the sample used for the calculation of the spectrum at each grid point of the structure is selected to be $0.01L$ and $0.01\pi R$ for the axial and the circumferential direction, respectively. The evolutionary power spectra along the directions of the cylinder are plotted in Fig. 10. From this figure, it can be observed that the standard deviation varies substantially along the two directions of the cylinder, while the correlation length remains almost constant and equal to $b_1 \approx 0.6L$ for the axial and $b_2 \approx 0.06(2\pi R)$ for the circumferential direction. In addition, the evolutionary power spectrum seems to be uniformly modulated since, as depicted in Fig. 10, the frequency content remains the same, while from the statistical analysis of the measured imperfections it occurs that the assumption of normality is in accordance with the experimental data.

A.2. Validity of the procedure for modeling the uncertain boundary conditions

The procedure for modeling the uncertainty on the boundary conditions via the non-uniformity of the axial loading, assuming that the two phenomena are essentially equivalent, can be supported by the following: a flatness survey of one of the loading end rings used in a test setup of a stiffened axially compressed anisotropic cylinder was presented in Arbocz (2000). The results of this survey are depicted in Fig. 11, where a plot of the trace of the corresponding imperfections at the cylinder's edges is shown. It is clear that the edge is non-uniformly loaded, due to the in-

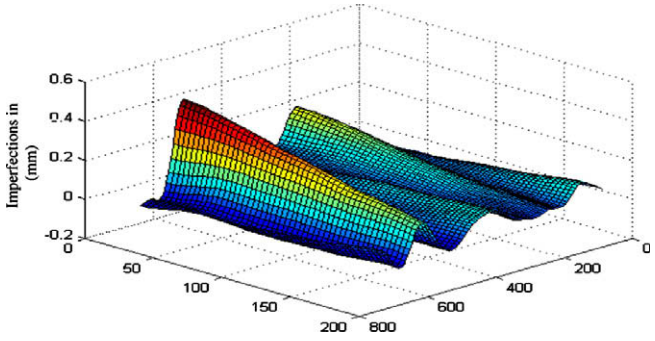

Fig. 8. Measured initial unfolded shape of shell A7.

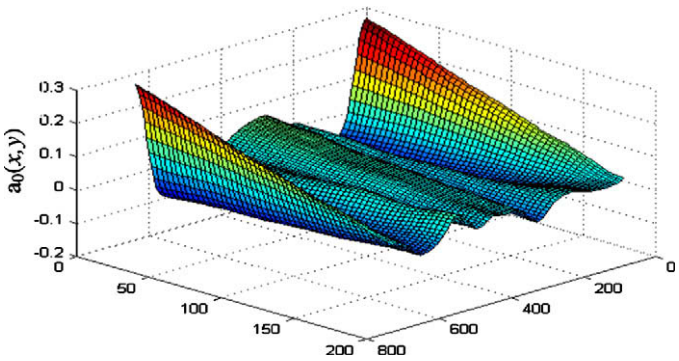

Fig. 9. Ensemble average of initial imperfections.

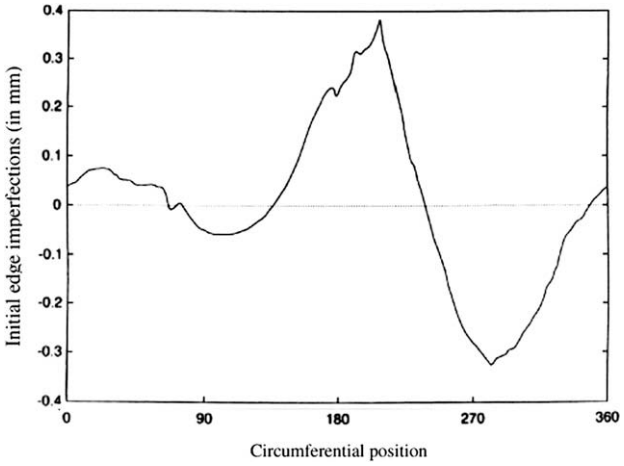

Fig. 11. Measured flatness of the end ring in Arbocz (2000).

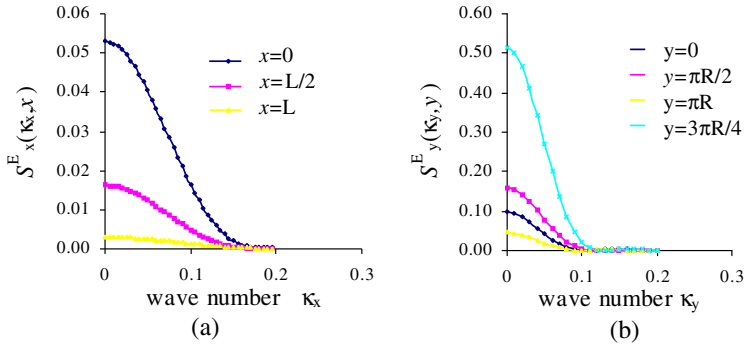

Fig. 10. Evolutionary power spectra along the: (a) axial direction and (b) circumferential direction of the cylinder.

plane geometric imperfections which do not allow a complete and solid contact between the cylinder and the loading member. As a result, the vertical load is applied as a series of point forces, non-uniformly distributed along the deformed edges of the cylinder. Thus, using the proposed approach, the following effects are taken into account in the modeling: (i) non-uniformity of the end loads acting on both edges of the cylinder, (ii) contribution of the edge imperfections to the overall pre-buckling deformations, (iii) rotation of the end loading plates, usually observed in the experiments, which is indirectly represented with the overall bending moment introduced by the non-uniformity of the vertical loads and, (iv) vertical misalignment of the end loads which is directly related to the upper and lower out-of-plane edge imperfections. A detailed description of the aforementioned approach and further justification of its validity can be found in Papadopoulos and Iglesis (2007).

References

Arbocz, J., 2000. The effect of imperfect boundary conditions on the collapse behavior of anisotropic shells. International Journal of Solids and Structures 37, 6891–6915.

Arbocz, J., Abramovich, J.H., 1979. The initial imperfection data bank at the Delft University of Technology, Part 1. Report LR-290, Department of Aerospace Engineering, Delft University of Technology.

Arbocz, J., Starnes Jr., J.H., 2002. Future directions and challenges in shell stability analysis. Thin-Walled Structures 40 (9), 729–754.

Argyris, J., Papadrakakis, M., Karapitta, L., 2002a. Elastoplastic analysis of shells with the triangular element TRIC. Computer Methods in Applied Mechanics and Engineering 191 (33), 3613–3637.

Argyris, J., Papadrakakis, M., Stefanou, G., 2002b. Stochastic finite element analysis of shells. Computer Methods in Applied Mechanics and Engineering 191 (41–42), 4781–4804.

Argyris, J., Tenek, L., Papadrakakis, M., Apostolopoulou, C., 1998. Post-buckling performance of the TRIC natural mode triangular element for isotropic and laminated composite shells. Computer Methods in Applied Mechanics and Engineering 166 (3–4), 211–231.

Bielewicz, E., Górski, J., 2002. Shells with random geometric imperfections: simulation-based approach. International Journal of Non-Linear Mechanics 37 (4–5), 777–784.

Choi, C.K., Noh, H.C., 2000. Stochastic analysis of shape imperfections in RC cooling tower shells. Journal of Structural Engineering (ASCE) 126 (3), 417–423.

Chryssanthopoulos, M.K., Poggi, C., 1995. Probabilistic imperfection sensitivity analysis of axially compressed composite cylinders. Engineering Structures 17 (6), 398–406.

Deml, M., Wunderlich, W., 1997. Direct evaluation of the 'worst' imperfection shape in shell buckling. Computer Methods in Applied Mechanics and Engineering 149 (1–4), 201–222.

Deodatis, G., Micaletti, R.C., 2001. Simulation of highly skewed non-Gaussian stochastic processes. Journal of Engineering Mechanics (ASCE) 127 (12), 1284–1295.

Elishakoff, I., 2000. Uncertain buckling: its past, present and future. International Journal of Solids and Structures 37 (46–47), 6869–6889.

Elishakoff, I., Li, Y.W., Starnes Jr, J.H., 2001. Non-Classical Problems in the Theory of Elastic Stability. Cambridge University Press. pp. 137–174.

Graham, L.L., Siragy, E.F., 2001. Stochastic finite element analysis for elastic buckling of stiffened panels. Journal of Engineering Mechanics (ASCE) 127 (1), 91–97.

Grigoriu, M., 1984. Crossings of non-Gaussian translation processes. Journal of Engineering Mechanics (ASCE) 110 (4), 610–620.

Grigoriu, M., 1998. Simulation of stationary non-Gaussian translation processes. Journal of Engineering Mechanics (ASCE) 124 (2), 121–126.

Ikeda, K., Murota, K., 2008. Asymptotic and probabilistic approach to buckling of structures and materials. Applied Mechanics Reviews (ASME) 040801. 16pp.

Koiter, W.T., 1963. The effects of axisymmetric imperfections on the buckling of cylindrical shells under axial compression. Proceedings of Royal Netherlands Academy of Sciences 66 (B), 265–279.

Lagaros, N.D., Papadopoulos, V., 2006. Optimum design of shell structures with random geometric, material and thickness imperfections. International Journal of Solids and Structures 43 (22–23), 6948–6964.

Lagaros, N.D., Stefanou, G., Papadrakakis, M., 2005. An enhanced hybrid method for the simulation of highly skewed non-Gaussian stochastic fields. Computer Methods in Applied Mechanics and Engineering 194 (45–47), 4824–4844.

Li, C.C., Der Kiureghian, A., 1992. An optimal discretization of random fields. Technical Report UCB/SEMM-92/04, Department of Civil Engineering, University of Berkeley, CA, USA.

Morris, N.F., 1996. Shell stability: the long road from theory to practice. Engineering Structures 18 (10), 801–806.

Noh, H.C., 2006. Effect of multiple uncertain material properties on the response variability of in-plane and plate structures. Computer Methods in Applied Mechanics and Engineering 195 (19–22), 2697–2718.

Onkar, A.K., Upadhyay, C.S., Yadav, D., 2006. Generalized buckling analysis of laminated plates with random material properties using stochastic finite elements. International Journal of Mechanical Sciences 48 (7), 780–798.

Palassopoulos, G.V., 1993. New approach to buckling of imperfection-sensitive structures. Journal of Engineering Mechanics (ASCE) 119, 850–869.

Papadopoulos, V., Iglesis, P., 2007. The effect of non-uniformity of axial loading on the buckling behavior of shells with random imperfections. International Journal of Solids and Structures 44 (18–19), 6299–6317.

Papadopoulos, V., Papadrakakis, M., 2004. Finite element analysis of cylindrical panels with random initial imperfections. Journal of Engineering Mechanics (ASCE) 130 (8), 867–876.

Papadopoulos, V., Papadrakakis, M., 2005. The effect of material and thickness variability on the buckling load of shells with random initial imperfections. Computer Methods in Applied Mechanics and Engineering 194 (12–16), 1405–1426.

Schenk, C.A., Schuëller, G.I., 2003. Buckling analysis of cylindrical shells with random geometric imperfections. International Journal of Non-Linear Mechanics 38 (7), 1119–1132.

Schenk, C.A., Schuëller, G.I., 2007. Buckling analysis of cylindrical shells with cut-outs including random boundary and geometric imperfections. Computer Methods in Applied Mechanics and Engineering 196 (35–36), 3424–3434.

Shinozuka, M., Deodatis, G., 1996. Simulation of multi-dimensional Gaussian stochastic fields by spectral representation. Applied Mechanics Reviews (ASME) 49 (1), 29–53.

Stefanou, G., Papadrakakis, M., 2004. Stochastic finite element analysis of shells with combined random material and geometric properties. Computer Methods in Applied Mechanics and Engineering 193 (1–2), 139–160.

Tsouvalis, N.G., Zafeiratou, A.A., Papazoglou, V.J., 2003. The effect of geometric imperfections on the buckling behavior of composite laminated cylinders under external hydrostatic pressure. Composites Part B: Engineering 34, 217–226.